Inorganica Chimica Acta 522 (2021) 120352

Contents lists available at ScienceDirect

Inorganica Chimica Acta

journal homepage: www.elsevier.com/locate/ica

Research paper

The Co(II), Ni(II), Cu(II) and Zn(II) complexes of aroylhydrazone of quinolone core: Syntheses, characterization and evaluation of antimicrobial and antitubercular activity

Ganesh S. Hegde [a,b], Satish S. Bhat [a], Sandeep P. Netalkar [a], Pooja L. Hegde [a], Avinash Kotian [a], Ray J. Butcher [c], Vidyanand K. Revankar [a,*]

[a] Department of Chemistry, Karnatak University, Pavate Nagar, Dharwad 580 003, Karnataka, India
[b] Department of Chemistry, M. E. S., M. M. Arts & Science College, Sirsi, Uttara Kannada 581402, Karnataka, India
[c] Department of Chemistry, Howard University, Washington, DC 20059, USA

ARTICLE INFO

Keywords:
Quinolone
Antimicrobial
Antituberculosis
Single-crystal X-ray diffraction

ABSTRACT

The ligand 3,5-di-*tert*-butyl-2-hydroxy-*N*'-((2-oxo-1,2-dihydroquinolin-3-yl)methylene)benzohydrazide (**H_2L**) and its Co(II), Ni(II), Cu(II), Zn(II) complexes were synthesized. The ligand and its complexes were characterized by various spectro-analytical techniques including IR, ^{1}H NMR, ^{13}C NMR, EPR, electronic spectroscopy, and elemental analysis. In addition, the molecular structures of H_2L, $[Co^{II}(HL)_2]$ **(1)**, $[Ni^{II}(HL)_2]$ **(2)**, $[Cu^{II}(HL)(Cl)(CH_3OH)]$ **(3)**, and $[Cu^{II}(HL)(H_2O)(CH_3OH)].ClO_4$ **(4)** were unambiguously established using single-crystal X-ray structure determination. However, the Zn(II) complex was characterized based on the IR, NMR and elemental analysis and the 6-coordinate with a 1:2 (M:L) ratio was proposed with the molecular formula $[Zn^{II}(HL)_2]$ **(5)**. The synthesized compounds were investigated for antimicrobial and antitubercular activities. The copper(II) complex **4**, has shown the lowest MIC of 0.4 μg/mL, against the gram-positive *S. Aureus* microorganism, which was better than the ligand and the standard *Ciprofloxacin* drug. Except for the complex **3**, the ligand and rest of its complexes exhibited better activity against gram-negative, *E. Coli* with the MIC values ranging from 0.4 – 0.8 μg/mL and were much better than the standard *Ciprofloxacin* drug

1. Introduction

Multifunctional heterocyclic compounds play important roles in drug discovery and developments with over 50% of the pharma market drugs containing heterocyclic ring systems [1]. Tuberculosis (TB) is a major disease mainly caused by *Mycobacterium tuberculosis* (MTB), and the other species of bacteria triggering tuberculosis are *M. africanum, M. pinnipedii, M. bovis, M. canettii, M. microti* and *M. caprae* [2]. In recent years, drug resistant tuberculosis is a worldwide public health problem [3]. Investigators throughout the world have been concerned about the wide spread of the tuberculosis disease due to their developed drug resistance towards existing drugs. Hence, there is urgent need to design and develop new drug molecules with an alternative mechanism of action. Several literature reports have revealed that molecules derived from quinolone hydrazones exhibit excellent anti-TB properties [4-8]. The hydrazone derivatives of quinolones contain both polar and non-polar groups, which makes them suitable for permeation into the bacterial cell [2]. This research finding indicates that the improved activity of quinolone hydrazones is due to their enhanced amphiphilic properties and solubilities, leading to the penetration of hydrazones into the cell wall of the *M. tuberculosis* [2,3]. The mechanism of anti-TB activity of quinolone hydrazones might be by interaction with the DNA gyrase enzyme. The interaction of metal complexes with DNA gyrase inhibits the multiplication of bacterial cells, leading to the death of the bacteria [2,3,9,10]. Among all the ligand systems, quinolone hydrazone derivatives are one of the most important due to its diverse chelating ability, structural flexibility, and broad-spectrum of biological activities, such as antifungal [11], antimalarial [12], anti-bacterial [13], anticonvulsant and analgesic activity [14]. In addition, the quinolone scaffold is privileged in the cancer drug discovery [15]. Recently, Mandewale *et al.* have reported the antitubercular activity of hydrazone derivatives of quinolone and their Zn(II) complexes where the activity of these complexes is comparable to "first and second line" drugs used to treat tuberculosis [3]. Liu *et al.* reported novel quinolone hydrazones and

* Corresponding author.
E-mail address: vkrevankar@rediffmail.com (V.K. Revankar).

https://doi.org/10.1016/j.ica.2021.120352
Received 6 October 2020; Received in revised form 7 March 2021; Accepted 9 March 2021
Available online 16 March 2021

their Cu(II) complexes that interact with CT-DNA by an intercalation mechanism [16]. Creaven *et al.* reported the Cu(II) complexes of quinolone hydrazone derivatives having good anticancer activity against the Hep-G2 cell line [17].

The above discussed results encouraged us to design Schiff base metal complexes using an aroylhydrazone derived from 2-oxo-1,2-dihydroquinoline-3-carbaldehyde to investigate their antimicrobial and antituberculosis activity studies. In the present work, we report the syntheses, structural characterization, antimicrobial and antitubercular activity of 3,5-di-*tert*-butyl-2-hydroxy-*N'*-((2-oxo-1,2-dihydroquinolin-3-yl)methylene) benzohydrazide (**H_2L**) and its Co(II), Ni(II), Cu(II), Zn (II) complexes. The molecular structures of H_2L, $[Co^{II}(HL)_2]$ **(1),** $[Ni^{II}(HL)_2]$ **(2)**, $[Cu^{II}(HL)(Cl)(CH_3OH)]$ **(3),** and $[Cu^{II}(HL)(H_2O)(CH_3OH)].ClO_4$ **(4)** were unambiguously established using single-crystal X-ray structure determination. The synthesized compounds were investigated for antimicrobial and antitubercular activities.

2. Experimental

The chemicals used were of reagent grade. Purified solvents were used for the syntheses of ligand and complexes.

2.1. Methods and instrumentations

The FTIR spectra were recorded in a KBr disc matrix using an Impact-410 Nicolet (USA) FTIR spectrometer over the range of 4,000–400 cm^{-1}. C, H, N elements were determined on the Elementar Vario EL III CHN analyzer. The ^1H and ^{13}C NMR spectra were recorded on Agilent 400MR DD2 spectrometer, in $CDCl_3$ (^1H NMR: 400 MHz, ^{13}C NMR: 100 MHz) at room temperature. EPR spectra of copper(II) complexes were recorded on Varian E–4 X-band EPR spectrometer, using TCNE as the < g > marker. The electronic spectra were measured on a Hitachi 150–20 spectrophotometer over the range of 800–200 nm. The molar conductance measurements were made on the ELICO–CM–82 conductivity bridge and were measured in DMF / $CHCl_3$ solution with 10^{-3} M concentration.

2.2. Synthesis of the Schiff base ligand (H_2L)

The 2-oxo-1,2-dihydroquinoline-3-carbaldehyde [16,18] and 3,5-di-*tert*-butyl-2-hydroxybenzohydrazide [19] were prepared as per the procedures mentioned in the reported literatures. 3,5-di-*tert*-butyl-2-hydroxybenzohydrazide (1.322 g, 0.005 mol) taken in methanol (30 mL) was treated with 2-oxo-1,2-dihydroquinoline-3-carbaldehyde (0.866 g, 0.005 mol) taken in a round-bottomed flask. The reaction mixture was stirred at room temperature for nearly an hour, until the yellowish precipitate resulted, Scheme 1**.** The reaction product was then filtered off, dried and recrystallized from methanol resulting in the formation of the ligand, **H_2L.**

Yield: 1.468 g, (70%); M.P. (°C): >300 °C; Anal. Calcd. for $C_{25}H_{29}N_3O_3$ (%): C, 71.58; H, 6.97; N, 10.02. Found (%): C, 71.56; H, 6.98; N, 10.15. FTIR, (cm^{-1}): C═O (1655), imine > C═N- (1636), OH (3472), NH (3219), C—O (1025), –CH (sp^2, sp^3) (2957, 2869). ^1H NMR (DMSO-d_6, 400 MHz, δ ppm): 13.09 (s, 1H, C(2)-phenolic OH), 12.05 (s, 1H, hydrazine NH), 12.08 (s, 1H, quinolone NH), 8.85 (s, 1H, –HC = N), 7.41 (s, 1H, C4H, aromatic), 7.76 (s, 1H, C6H, aromatic), 8.50 (s, 1H, C17H, aromatic), 7.32 (d, J = 8 Hz, 1H, C12H, aromatic), 7.19 (t, J = 8 Hz, 1H, C13H aromatic), 7.50 (t, J = 8 Hz, 1H, C14H aromatic), 7.86 (d, J = 8 Hz, 1H, C15H, aromatic), ^{13}C NMR (DMSO-d_6, 100 MHz, δ ppm): 29.6, 31.7, 34.7, 35.2 (t Bu), 161.5 (HC8 = N),168.1 (C7 = O), 158.9 (C10 = O), 144.9 (*C*2-OH phenolic), 140.2 and 139.6 (C1 and C9, aromatic), 119.4 and 125.4 (C3 and C5, aromatic), 136.9 and 135.8 (C4 and C6, aromatic), 131.9 (C11, aromatic), 129.7 and 128.8 (C12 and C17, aromatic), 122.9 and 121.9 (C13 and C14, aromatic), 115.6 and 112.7 (C15 and C16, aromatic). UV–Vis ($CHCl_3$): λ_{max} (nm), (ε_{max}($Lmol^{-1}cm^{-1}$)): 380(10,820), 406(5,753).

2.3. General procedure for syntheses of the complexes

The hot methanolic solutions of the respective metal chlorides (2.5 mmol) were added dropwise with stirring to the ligand, **H_2L** (5 mmol) suspended in 35–40 mL of methanol, taken in round-bottomed flasks. After the complete addition of the metal(II) salt solution, the reaction mixtures were stirred for 30–40 min at 60–65 °C and refluxed for 3–4 h. For the syntheses of copper complexes 5 mmol of metal salts were used instead of 2.5 mmol. The isolated complexes were filtered in hot condition, washed with hot ethanol and dried.

2.3.1. Synthesis of $[Co^{II}(HL)_2]$ (1)

The synthesis of complex **1** was similar to that as described in the general procedure by using cobalt chloride hexahydrate (0.059 g, 2.5 mmol) and H_2L (0.209 g, 5 mmol). Yield: 0.145 g (65%); Anal. Calc. for $CoC_{50}H_{56}N_6O_6$ (%): C, 67.03; H, 6.30; N, 9.38 Found (%): C, 67.12; H, 6.41; N, 9.41. FTIR, (cm^{-1}): imine > C═N- (1595), >C═O (1632), OH (3389), –NH (3150), C—O (1079), –CH (sp^2, sp^3) (2957, 2868). Molar Cond. Λ_M(CH_3OH, mho cm^2 mol^{-1}): 10.4. UV–Vis (CH_3OH): λ_{max}(nm), (ε_{max}($Lmol^{-1}cm^{-1}$)): 230(11,601), 391(18,417).

2.3.2. Synthesis of $[Ni^{II}(HL)_2]$ (2)

The synthesis of complex **2** was similar to that as described in general

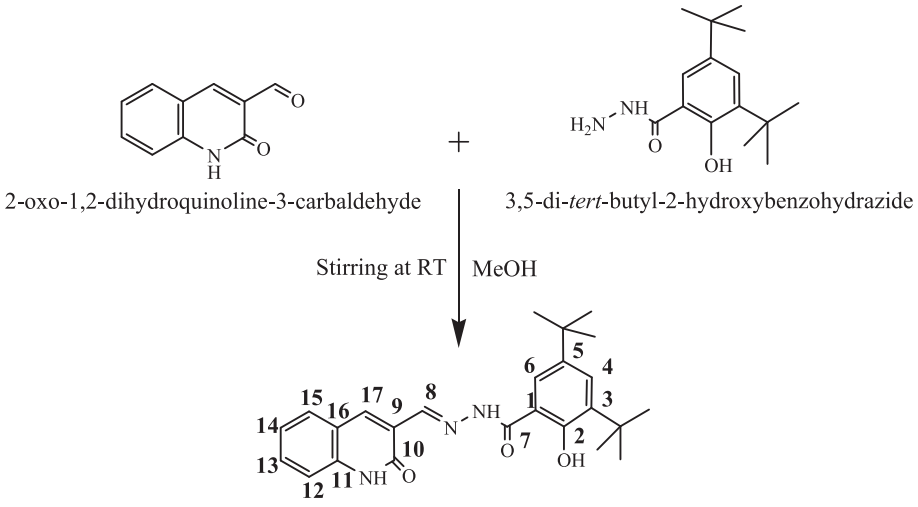

Scheme 1. The synthesis strategy of the ligand, **H_2L,** and its carbon numbering for the NMR interpretation.

procedure by using nickel chloride hexahydrate (0.059 g, 2.5 mmol) and H_2L 0.209 g, 5 mmol). Yield: 0.138 g (62%); Anal. Calc. for $NiC_{50}H_{56}N_6O_6$ (%): C, 67.05; H, 6.30; N, 9.38 Found (%): C, 66.91; H, 6.31; N, 9.32. FTIR, (cm^{-1}): imine > C═N- (1597), >C═O (1634), OH (3397), –NH (3150), C—O (1083), –CH (sp^2, sp^3) (2957, 2872). Molar Cond. Λ_M(CH_3OH, mho cm^2 mol^{-1}): 2.4. UV–Vis (CH_3OH): λ_{max}(nm), (ε_{max}($Lmol^{-1}cm^{-1}$)): 376(9,405), 395(12,765), 416(11,563), 750(19.3), 907(32.8).

2.3.3. Synthesis of $[Cu^{II}(HL)(Cl)(CH_3OH)].CH_3OH$ (3)

The synthesis of complex **3** was similar to that as described in the general procedure by using copper chloride dihydrate (0.085 g, 5 mmol) and H_2L (0.209 g, 5 mmol). Yield: 0.227 g (78%); Anal. Calc. for $CuC_{27}H_{36}N_3O_5Cl$ (%): C, 55.76; H, 6.24; N, 7.23; Cl, 6.10 Found (%): C, 55.63; H, 6.37; N, 7.35; Cl, 6.25. FTIR, (cm^{-1}): imine > C═N- (1593), >C═O (1639), OH (3413), C—O (1084), –CH (sp^2, sp^3) (2951, 2866). Molar Cond. Λ_M(CH_3OH, mho cm^2 mol^{-1}): 10.9. UV–Vis (CH_3OH): λ_{max}(nm), (ε_{max}($Lmol^{-1}cm^{-1}$)): 391(9,872), 407(9,085), 685(1 1 4). EPR ($g_{||}$, g⊥, Grnd. State, Geometry): 2.2639, 2.0710, d_{x2-y2}, Sq. Pyramidal.

2.3.4. Synthesis of $[Cu^{II}(HL)(H_2O)(CH_3OH)].ClO_4$ (4)

The synthesis of complex **4** was similar to that as described in general procedure by using copper perchlorate hexahydrate (0.185 g, 5 mmol) and H_2L (0.209 g, 5 mmol). Yield: 0.236 g (75%); Anal. Calc. for $CuC_{26}H_{34}ClN_3O_9$ (%): C, 49.44; H, 5.43; N, 6.65; Cl, 5.61 Found (%): C, 49.52; H, 5.48; N, 6.76; Cl, 5.69. FTIR, (cm^{-1}): imine > C═N- (1594), >C═O (1636), –NH (3201), OH (3445), C—O (1085), –CH (sp^2, sp^3) (2955, 2863). Molar Cond. Λ_M(CH_3OH, mho cm^2 mol^{-1}): 101.6. UV–Vis (CH_3OH): λ_{max}(nm), (ε_{max}($Lmol^{-1}cm^{-1}$)): 390(4,988), 408(4,562), 675 (1 1 5). EPR ($g_{||}$, g⊥, Grnd. State, Geometry): 2.2155, 2.0562, d_{x2-y2}, Sq. Pyramidal.

2.3.5. Synthesis of $[Zn^{II}(HL)_2)]$ (5)

The synthesis of complex **5** was similar to that as described in general procedure by using zinc chloride hexahydrate (0.061 g, 2.5 mmol) and H_2L (0.209 g, 5 mmol). Yield: 0.146 g (65%); Anal. Calc. for $ZnC_{50}H_{56}N_6O_6$ (%): C, 66.55; H, 6.26; N, 9.31 Found (%): C, 66.39; H, 6.37; N, 9.28. FTIR, (cm^{-1}): imine > C═N- (1598), >C═O (1641), OH (3440), C—O (1083), –CH (sp^2, sp^3) (2955, 2866). Molar Cond. Λ_M(CH_3OH, mho cm^2 mol^{-1}): 5.72. ^{1}H NMR (DMSO-d_6, 400 MHz, δ ppm) : 14.37 (s, 1H, C(2)-phenolic OH), 13.11 (s, 1H, hydrazine NH), 3.88 (s, 1H, quinolone NH), 8.84 (s, 1H, –HC = N), 7.36 (s, 1H, C4H, aromatic), 7.69 (s, 1H, C6H, aromatic), 8.57 (s, 1H, C17H, aromatic), 7.25 (d, J = 3 Hz, 1H, C12H, aromatic), 7.34 (t, J = 3 Hz, 1H, C13H aromatic), 7.65 (t, J = 8 Hz, 1H, C14H aromatic), 7.84 (d, J = 8 Hz, 1H, C15H, aromatic), ^{13}C NMR (DMSO-d_6, 100 MHz, δ ppm): 29.7, 31.6, 34.3, 35.1 (t Bu), 157.7 (HC8 = N),173.2 (C7 = O), 146.4 (C10 = O), 138.8 (*C*2-OH phenolic). UV–Vis (CH_3OH): λ_{max}(nm), (ε_{max}($Lmol^{-1}cm^{-1}$)): 388(9,673), 419(5,231).

2.4. Single crystal X-ray diffraction

Single crystals of **H_2L**, **3** and **4** were obtained by the slow evaporation of the compound in methanol, whereas single crystals of the complex, **1** and **2** were obtained by the slow evaporation of the complex in dimethylformamide at room temperature.

Single crystal data of ligand **H_2L** and **1** was collected on a Bruker SMART X2S bench top crystallographic system. The Single crystal data for **2** was collected on Bruker d8 Venture diffractometer. The single crystal data of complexes **3** and **4** was collected on Bruker AXS Kappa Apex2 diffractometer. Intensity measurements were performed using monochromated (doubly curved silicon crystal) Mo-Kα radiation (0.71073 Å) from a sealed micro focus tube. Generator settings were 50 kV, 1 mA. APEX2 software was used for the preliminary determination of the unit cell. Determination of integrated intensities and unit cell refinement were performed using SAINT [20]. The data was corrected for absorption effects with SADABS [20] using the multiscan technique. The structure was resolved on Olex2.0 [21] package using ShelxT [22] and refined by full-matrix least squares based on F^2, using ShelxL [22]. Badly disordered solvents molecules in the lattice of **H_2L** could not be resolved and were removed using the SQUEEZE routine from Platon [23]. The complex **1** contains four disordered *tert-butyl* and two DMF molecules, while the complex **2** contains whole molecule disorder for one ligand and partial disorder for the other two DMF molecules. Similarly, complex **3** contains disordered *tert-butyl* and methanol, while complex **4** contains disordered *tert-butyl* and ClO_4^- anion. H-atom positions were calculated geometrically and refined using a riding model. For complexes **3** and **4** the H atoms for the coordinated methanol were located in difference Fourier and refined using a riding model. The CCDC 2031315, 2031312, 2031316, 2031313, 2031314 contains the supplementary crystallographic data for **H_2L**, **1**, **2**, **3**, and **4** respectively for this paper. The crystallographic parameters of these complexes were tabulated in the Table 1.

2.5. Biological protocols

2.5.1. Antimicrobial activity

All the synthesized compounds were evaluated for their antimicrobial activity against *Staphylococcus aureus* gram-positive bacterium and *Escherichia coli* gram-negative pathogens using the micro broth dilution method [24,25] Ciprofloxacin was used as the standard drug to compare the activity of the samples and the Minimum Inhibitory Concentration (MIC) for both the pathogens is 2 μg/mL. The potency of the ligand and its complexes was studied by comparing the turbidity formed with that of the standard drug on two bacterial strains.

2.5.2. Antitubercular activity

The synthesized compounds were also evaluated for their antimycobacterial activities against *M. tuberculosis* (H37 RV strain): ATCC No– 27294, using the Microplate Alamar Blue Assay (MABA) method [24].

3. Results and discussion

3.1. Syntheses and characterization

The ligand, **H_2L** was synthesized by the reaction of 3,5-di-*tert*-butyl-2-hydroxybenzohydrazide with 2-oxo-1,2-dihydroquinoline-3-carbaldehyde in methanol (Scheme 1.) and was characterized by IR, NMR and elemental analysis etc. (see the Experimental Section). The complexes, **1**–**5** were synthesized in good yields by refluxing **H_2L** and metal salts in methanol in appropriate ratios. The purity of the compounds was confirmed by elemental analysis, and IR Spectroscopy (see the Experimental Section). The ligand and its complexes, except **5**, were crystalline and single crystals were grown by the slow evaporation of their solutions either in methanol or in the mixture of methanol and dimethylformamide (DMF).

The FT-IR spectrum of the ligand, **H_2L** (**Fig. S1**), confirms the quinolone keto form, as the peaks at 1655 and 3219 cm^{-1} were due to > C═O and > NH absorptions respectively, which is also supported by the crystal structure of **H_2L**. The intense ligand peak at 1655 cm^{-1} with the shoulder at 1636 cm^{-1} for **H_2L** were ascribed to the > C═O and > C═N stretching frequencies respectively. Upon complexation, these bands shifted by 10 – 30 cm^{-1} in all the complexes indicating their coordination to metal ion [26]. The > NH stretching and C–NH bending absorptions at around 3150–3200 and 1552–1566 cm^{-1} respectively were found in most of these complexes. This suggested the coordination of either quinolone or amidic carbonyl without deprotonation [27]. The comparison of important FT-IR peaks of **H_2L** and its metal complexes are recorded in the Table S1. The ligand **H_2L** and its zinc(II) complex (**5**) were characterized by ^{1}H and ^{13}C NMR, and all the peaks were assigned (Tables S2 and S3; **Fig. S7-S10**). In the ^{1}H NMR spectrum of ligand **H_2L**,

Table 1
Crystal data and structure refinement details of the compounds.

Crystal data	1	2	3	4
Empirical formula	$C_{50}H_{56}CoN_6O_6{\cdot}4(C_3H_7NO)$	$C_{50}H_{56}N_6NiO_6{\cdot}\ 4(C_3H_7NO)$	$C_{26}H_{32}ClCuN_3O_4{\cdot}CH_3OH$	$C_{26}H_{34}ClCuN_3O_9$
Formula weight	1188.32	1188.10	581.58	631.55
Temperature/K	296 (2)	296 (2)	296 (2)	296 (2)
Crystal system	Monoclinic	Monoclinic	Triclinic	Triclinic
Space group	*C*2/*c*	*C*2/*c*	*P*-1	*P*-1
a/Å	34.0230 (8)	33.6627 (12)	8.9778 (19)	8.9358 (8)
b/Å	17.4599 (4)	17.2757 (5)	9.722 (3)	10.217 (10)
c/Å	22.4472 (6)	22.1176 (8)	18.092 (4)	17.3655 (17)
α/°	90°	90°	92.679 (10)	94.531 (4)
β/°	99.679 (2)	99.937 (2)	97.038 (11)	94.926 (5)
γ/°	90°	90°	111.805 (11)	112.265 (4)
Volume/Å^3	13144.7 (6)	12669.5 (7)	1447.8 (6)	1451.1 (2)
Z	8	8	2	2
Radiation	Mo Kα (λ = 0.71073 Å)	Mo *K*α (λ = 0.71073 Å)	Mo *K*α (λ = 0.71073 Å)	Mo *K*α (λ = 0.71073 Å)
Data/restraints/parameters	10,011 / 812 / 995	14531/2104 /1286	6552 / 123 / 400	6487/ 143 / 449
Goodness-of-fit on F^2	1.021	1.046	0.956	1.018
Final R indexes [I>=2σ (I)]	R1 = 0.0563 wR2 = 0.1479	R1 = 0.0676 wR2 = 0.1609	R1 = 0.0470, wR2 = 0.1024	R1 = 0.0418, wR2 = 0.1042
Final R indexes [all data]	R1 = 0.0886, wR2 = 0.1693	R1 = 0.1410 wR2 = 0.1925	R1 = 0.0984, wR2 = 0.1221	R1 = 0.0643, wR2 = 0.1153
Largest diff. peak/hole /e Å^{-3}	0.42 and − 0.65	0.722 and −0.590	0.47 and −0.29	0.33 and −0.39

the peak at 8.85 confirms the formation of the ligand through the imine linkage [28]. This imine proton exhibiting a slight shift of around 0.01 ppm in the zinc(II) complex indicate the coordination through this group [29]. The ^{1}H NMR spectrum of the zinc(II) complex of **H_2L** exhibited peaks at 8.83, 14.37, 13.11 and 3.88 ppm, which were assignable to imine, intramolecular hydrogen-bonded C(2)–OH, quinolone –NH and hydrazine –NH respectively, in the 1:2 M:L complex. These peaks have undergone significant shift compared with its ligand peaks. The ^{13}C NMR peak at 161 ppm was due to HC(8) = N azomethine carbon atom of the ligand. The appearance of this signal is the major supporting evidence for the successful formation of the ligand. The signals of ^{13}C NMR spectrum of the ligand observed at 159 and 168 ppm were assigned to the quinolone > C=O and –HN-C(7) = O carbon atoms, respectively. These peaks have undergone a slight shift in the complex because of the variations in the electron density due to the coordination of the neighboring oxygen atoms [30]. The other aromatic and aliphatic carbons were observed in the expected region and are detailed in Table S3. ^{13}C NMR spectra of ligand and its zinc complex are given in the **Fig. S8 and S10** respectively. Thus, the ligand in the zinc complex utilizes quinolone–O, azomethine –N and amidic carbonyl–O, respectively as donor sites while coordinating with the metal ion.

3.2. Single-Crystal X-ray diffraction studies

The structures of the **H_2L** and its complexes [Co^{II}(HL)$_2$] (**1**), [Ni^{II}(HL)$_2$] (**2**), [Cu^{II}(HL)Cl(CH$_3$OH)] (**3**) and [Cu^{II}(HL)(H$_2$O)(CH$_3$OH)]ClO$_4$ (**4**) were unambiguously established by X-ray diffraction studies.

3.2.1. Crystal Structure of H_2L

Single crystals of **H_2L** were obtained by the slow evaporation of ligand solution in methanol. Crystal of **H_2L** diffracted poorly, nevertheless we were able to obtain the structure of the ligand from the data collected. Badly disordered solvents molecules in the lattice could not be resolved and were removed using the SQUEEZE routine from Platon [23]. The Oak Ridge Thermal Ellipsoidal Plot (ORTEP) diagram of the **H_2L** is given in Fig. 1. The crystallographic and the geometric parameters are given in Table S4. The asymmetric unit was found to consist of two molecules. The packing diagram of the **H_2L** shows intermolecular as well as intramolecular hydrogen bonding as shown in the **Fig. S11**. During complexation, the ligand **H_2L** undergoes C—C single bond rotations at C17-C16 and C15-C6 to result into the suitable conformation so that it's ONO ligating sites orient towards the metal center.

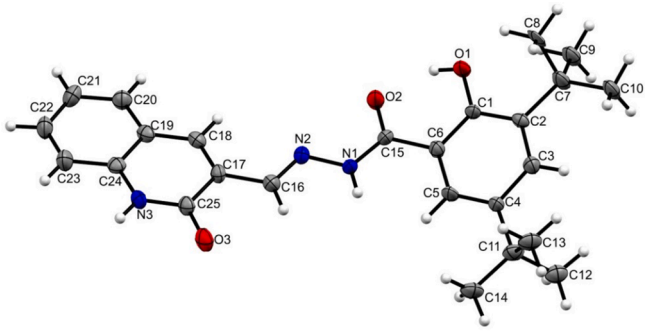

Fig. 1. ORTEP diagram of H_2L showing 20% probability ellipsoids.

3.2.2. Crystal Structures of [Co^{II}(HL)$_2$] (1) and [Ni^{II}(HL)$_2$] (2)

Single crystals of the complex, **1** and **2** were obtained by the slow evaporation of the complexes in dimethylformamide. The ORTEP diagrams of the complexes, **1** and **2** with 30% ellipsoidal probability are given in the Fig. 2 & **Fig. S12**, respectively. Both the complexes were crystallized in the *C*2/*c* space group in the monoclinic crystal system along with four molecules of dimethylformamide as solvent of crystallization. In complexing to Co (and the other metals in the complexes **2**, **3**, and **4**), the ligand, **H_2L**, has lost its N—H proton to be a uninegative (**HL**$^-$) species. The prominent bond length and bond angle data are provided in the **Tables 2, S5, 3 & S7** respectively. The packing diagrams of the crystal structures are given in **Fig. S13 and S14**. The X-ray crystal structures of **1** and **2** exhibited the distorted octahedral structures in which the metal ions (Co(II) and Ni(II)) are surrounded by the N_2O_4 coordination sphere, provided by the two tridentate ligands using quinolone-carbonyl-O, imine-N, and enolate-O of the amide group as donor sites arranged in the meridional fashion with the dihedral angles of 88.41° (as representatively shown in the **Fig. S15**) and 87.54°, respectively. The ONO donor sites of the tridentate ligands coordinate to the metal centers to form five and six membered chelate rings, with the bite angles of 77.2(1)° and 85.6(1)° respectively for the cobalt complex **1**, and 78.83(9)° and 87.8(1)°, respectively, for the nickel complex **2**, in one of their ligand parts indicating the distortion from the ideal octahedral geometry. The Co-O bond distances of the six-membered chelate rings [Co1-O1: 2.105(2) Å and Co1-O5: 2.095(3) Å] are slightly longer than those of the five-membered chelate rings [Co1-O2: 2.080(2) Å and Co1-O4: 2.080(2) Å] in the complex **1**. However, this trend is not clearly

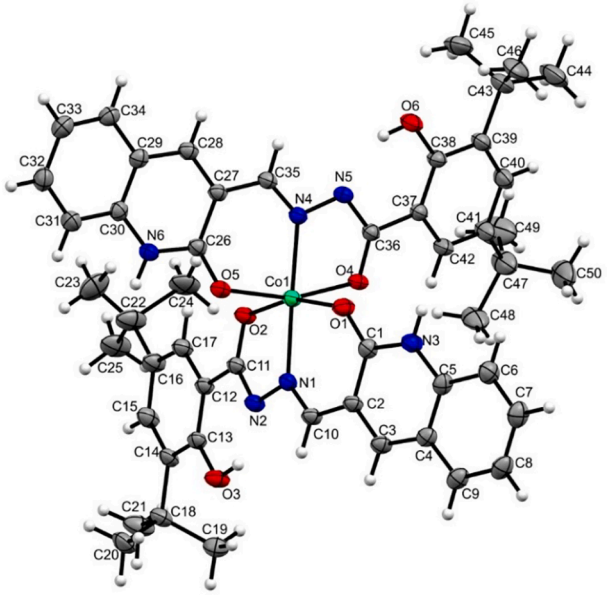

Fig. 2. ORTEP projection of **1** showing 20% probability ellipsoids, solvent molecules are omitted for clarity.

exhibited in the complex **2**, (six-membered chelate rings [Ni1-O6: 2.071 (2) Å and Ni1-O3: 2.155 (12) Å] and five-membered chelate rings [Ni1-O5: 2.075 (2) Å and Ni1-O2: 1.995 (7) Å]).

The bond lengths between metal and imine nitrogen donors of the two ligands in both the complexes slightly differ and were found to be Co1-N1: 2.074(3) and Co1-N4: 2.063(3) Å, and Ni1-N5: 1.996 (2) and Ni1-N2: 1.981 (9), respectively.

The Table S5 represents the comparative bond-length data of the bonds comprising the ligating atoms, in the free ligand, and in its complexes. When all the benzoylhydrazone carbonyl bond lengths of both the complexes are compared with that of the ligand's, they were found to have sufficiently elongated. This observation clearly supports the formation of coordination bond via enolate oxygen of the amidic group to the metal centers [31-33]. However, the quinoline parts of the ligands in both the complexes exist in the quinolone tautomeric forms, and coordinated with the carbonyl oxygen which is further supported by the shorter C═O distances as depicted in the Table S5 [34]. Among the 1:2 (M:L) complexes of cobalt and nickel, the geometrical data indicates that both the ligand parts in the cobalt complex show almost similar values, however, nickel complex exhibits quite larger variations may be due to the disordered ligands coordinated to the nickel.

3.2.3. *Crystal structure of* $[Cu^{II}(HL)Cl(CH_3OH)]$ (3)

The single crystals of copper complex **3** were grown by slow evaporation of the complex in methanol at room temperature. The ORTEP diagram of **3** along with atom labeling is shown in Fig. 3, the important bond parameters are compiled in the Tables 2, 3 and S5-S7**.** The complex, **3** was crystallized in the *P*-1 space group in the triclinic crystal system along with the methanol as solvent of crystallization. The copper coordination center in the crystal structure of **3** is five coordinate with a distorted square pyramidal geometry using NO_3Cl as donor atoms [τ_5 = 0.064] [35].

The ligand in the complex **3** was found to be monobasic tridentate utilizing quinolone oxygen-O, imine-N, and amidic enolate-O as ligating atoms. Complex **3** exhibited the coordination of one chlorine atom to the metal ion, which satisfies one more primary valency of the metal, and the fifth coordination was found to be satisfied by the oxygen of the methanol solvent molecule. The ONO donor sites of the tridentate ligand in **3** coordinate the Cu(II) center to form one six-membered and the other five-membered chelate rings, with the bite angles of 91.63(9)° and

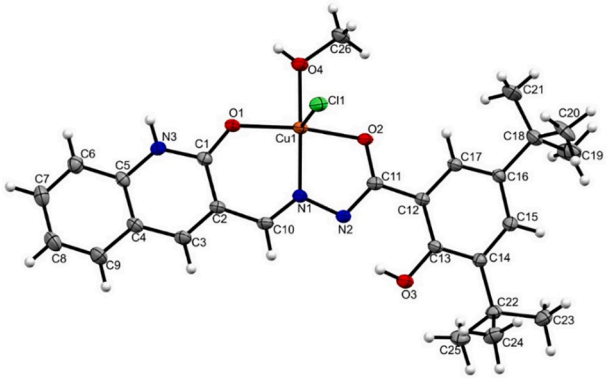

Fig. 3. ORTEP projection of **3** showing 20% probability ellipsoids, solvent molecule is omitted for clarity.

81.8(9)° respectively. The chelate rings lie in two slightly different planes with the dihedral angles of 9.16° as shown in **Fig. S16**. The average bond lengths [Cu–O and Cu–N] in the basal plane of the complex is 1.92 Å. However, the Cu-Cl apical bond distance is found to be longer with 2.556(1) and is comparable with those observed for the similarly reported complexes [36,37]. The copper atom is found to be displaced by 0.284 Å from the basal plane towards the apical chlorine, as observed in most of the square pyramidal complexes. The intramolecular hydrogen bonding between the phenolic proton of the aroyl benzene ring with the amidic nitrogen was observed in the complex. The packing diagram of complex, **3** (**Fig. S17**) exhibited the reciprocal hydrogen bonds between the apical chlorine with the coordinated methanol (2.26 Å) and crystal held methanol oxygens (3.28 Å) between the two complex molecules. The Cu-Cu distance was found to be 6.77 Å in this hydrogen-bonded dimeric unit. The ligand aromatic rings in each hydrogen-bonded dimer were involved in stacking interactions with the aromatic rings of the adjacent dimers.

3.2.4. *Crystal Structure of Complex* $[Cu^{II}(HL)(H_2O)(CH_3OH)]ClO_4$ (4)

The single crystals of **4** were obtained by the slow evaporation of the complex in methanol. The ORTEP diagram of **4** with 30% ellipsoidal probability is given in **Fig. S18.** The complex **4** crystallized in the triclinic crystal system with *P*-1 space group. The geometry around copper center is distorted square pyramidal geometry [$\tau_5 = 0.091$] [35]. The copper center is coordinated by monobasic tridentate ligand $\mathbf{HL}^-$ utilizing quinolone oxygen-O, imine-N, and amidic enolate-O as ligating atoms and the rest of the coordination sites were occupied equatorially by the methanol oxygen and the oxygen of a water molecule in the apical position. The positive charge of $[Cu(HL)(H_2O)(CH_3OH)]^+$ was balanced by the counter perchlorate ion present outside the coordination sphere.

The extended crystal structure of **4** exhibited the apical oxygen of the water molecule interacting with the coordinated methanol of the other molecule (1.92 Å) and with perchlorate oxygen (2.20 Å) present outside its coordination sphere. The two oxygen atoms of the perchlorate ion serve in extending the structure by connecting with the apical water molecule (as mentioned above) and the quinolone nitrogen (2.09 Å) of another molecule. Thus, each perchlorate and apical coordinated water belonging to one of the complexes connects two other complex molecules opposite to each other. This elongates the branching of the molecular assembly as shown in **Fig. S19**.

Apart from the hydrogen bonding interactions, the basal faces of the two such extended complexes are held by several stacking interactions between the aromatic rings. Thus, in the solid-state, the apical water and the perchlorate on the same side, extend the molecular connectivity like the staggered branches of a ladder and the bow like bent basal parts of the two complexes hold via stacking interactions appearing like the clapping hands as depicted in the **Fig. S20**. Such laddered array of molecules extends in other directions through the interactions between

Table 2
Prominent coordinated bond lengths (Å) for complexes **1**–**4**.

Complex	Metal-Quinoline carbonyl bond length		Metal-Imine nitrogen bond length		Metal-Benzoylhydrazone carbonyl bond length	
1	Co1–O5	Co1–O1	Co1–N4	Co1–N1	Co1–O4	Co1–O2
	2.095(3)	2.105(2)	2.063(3)	2.074(3)	2.080(2)	2.080(2)
2	Ni1–O6	Ni1–O3	Ni1–N5	Ni1–N2	Ni1–O5	Ni1–O2
	2.071(2)	2.155(12)	1.996(2)	1.981(9)	2.075(2)	1.995 (7)
3	Cu1–O1		Cu1–N1		Cu1–O2	
	1.934(2)		1.939(2)		1.928(2)	
	Other bond lengths :		Cu1–Cl1 2.556(1)	Cu1–O4 1.966(2)		
4	Cu1–O3		Cu1–N2		Cu1–O2	
	1.915(2)		1.928(2)		1.900(2)	
	Other bond lengths:		Cu1–O1W 2.445(3)	Cu1–O4 1.938(2)		

Table 3
Prominent bond angles (°) for complexes **1**–**4**.

Complex	Chelate ring bond angles (°)			
	Six membered Quinoline moiety		Five membered Benzoylhydrazone moiety	
1	N4–Co1–O5	N1–Co1–O1	O4–Co1–N4	O2–Co1–N1
	85.6(1)	85.5(1)	77.2(1)	76.8(1)
2	N5–Ni1–O6	N2–Ni1–O3	O5–Ni1–N5	O2–Ni1–N2
	87.8(1)	85.5(4)	78.83(9)	81.5(3)
3	N1–Cu1–O1		O2–Cu1–N1	
	91.63(9)		81.8(9)	
4	N2–Cu1–O3		O2–Cu1–N2	
	93.58(8)		82.11(8)	

one tertiary butyl group of one molecule with the others' and another *t-but* group with the methyl group of the coordinated methanol and thus forms the three-dimensional solid network.

3.3. Electronic spectral studies

The electronic spectra of the ligand and its complexes were recorded in methanol and the data summarized in Table 4. The representative spectra are shown in the Fig. S21. The ligand, **H_2L** showed an intense band with a sharp peak at 203 nm in methanol with low energy shoulders at 211 and 228 nm. These peaks remained almost the same in all the complexes of **H_2L**. Another band with a peak at 383 nm found along with both low and high energy side shoulders is assigned to the $\pi \rightarrow \pi^*$ and n $\rightarrow \pi^*$ electronic transitions of the ligand consisting large aromatic system comprising several functional groups like quinolone NH, quinolone carbonyl, imine, amide and phenolic groups. This band suffered a bathochromic shift in all the complexes indicating the involvement of these functional groups in the coordination sphere [30,38]. The electronic spectrum of the octahedral Co(II) complex **1** didn't exhibit any suitable peaks due to *d* – *d* electronic transitions in the visible range in support of its geometry, hence it couldn't be explored. The electronic spectrum of the Zn(II) (d^{10}) complex **5** exhibited a band in the region 380 – 419 nm with the ε in the range of 5000–10000 *L* cm^{-1} mol^{-1}, which was accounted for the ligand to metal charge transfer transition in the complex. The other bands appeared around 250 nm and above are attributed to the ligand bands.

Table 4
Electronic spectral data of the ligand and complexes.

Compound	λ_{max} (nm) (ε_{max}($Lmol^{-1}cm^{-1}$))	Compound	λ_{max} (nm) (ε_{max}($Lmol^{-1}cm^{-1}$))
H_2L	203(41,832), 211 (19,177), 228(11,283), 326(7,097), 344 (8,128), 380(10,820), 406(5,753)	[Cu^{II}(HL)(Cl)(CH_3OH)] (**3**)	204(20,614), 210 (12,514), 259(6,272), 349(6,133), 391 (9,872), 407(9,085), 685(114)
[$Co^{II}(HL)_2$] (**1**)	203(1,81,755), 216 (20,244), 230(11,601), 391(18,417)	[Cu^{II}(HL)(H_2O)(CH_3OH)].ClO_4 (**4**)	203(29,123), 210 (6,325), 260(2,845), 350(3,115), 390 (4,988), 408(4,562), 675(115)
[$Ni^{II}(HL)_2$] (**2**)	265(32,197), 376 (9,405), 395(12,765), 416(11,563), 750 (19.3), 907(32.8)	[$Zn^{II}(HL)_2$] (**5**)	206(27,347), 320 (2,118), 334(2,321), 388(9,673), 419(5,231)

The electronic spectra of octahedral nickel(II) (d^8) complexes in O_h symmetry generally have three spin-allowed transitions (Fig. S22). The assignments of those bands are as follows, $^3T_{2g} \leftarrow {}^3A_{2g}(\nu_1)$, $^3T_{1g} \leftarrow {}^3A_{2g}(\nu_2)$ and $^3T_{1g}(P) \leftarrow {}^3A_{2g}(\nu_3)$. The lowest energy band at 907 nm region is assigned to ν_1 [$^3T_{2g} \leftarrow {}^3A_{2g}$] transition and other bands at 750 and 416 nm region are assigned to ν_2 [(F) $^3T_{1g} \leftarrow {}^3A_{2g}$] and ν_3 [$^3T_{1g}(P) \leftarrow {}^3A_{2g}$] transitions, respectively. The appearance of three d-d bands for [$Ni^{II}(HL)_2$], **2**, made it possible for us to assign the octahedral geometry around nickel ion [39].

The electronic spectra of copper(II) complexes, **3** & **4** exhibited the λ_{max} values around 408 and 675–685 nm. These were the electronic transitions influenced by the coordinate bond. Because of the Jahn–Teller distortion and the low symmetry of the environment around Cu (II) d^9, detailed interpretations of the electronic spectra are quite complicated. Both the copper(II) complexes, **3** and **4** are dark green due to the presence of a broad absorption band with the peaks at 685 and 675 nm respectively, as shown in Fig. S23. Both of these were found to have square pyramidal geometry from their crystallographic studies as well as EPR spectral data.

3.4. EPR spectral studies

The EPR spectra are recorded for the copper complexes in the powder form and the results are presented in Table 5. The representative EPR spectra of the complexes are provided in the Fig. 4. The ground state orbital and the respective geometries for all the complexes were mentioned based on the corresponding 'g' values. The $g_{||}$ values less than 2.3 for both of the copper complexes indicate the larger percentage of covalency in their metal–ligand bonds [40].

The geometric parameter G is the measure of the exchange interaction between the copper centers in polycrystalline solid, which can be calculated using the equation: $G = (g_{||} - 2.0023) / (g_{\perp} - 2.0023)$. This value of G if less than 4 indicates the considerable exchange interaction in the crystalline compound and if $G > 4$, the exchange interaction is negligible. The calculated values of G for the complexes, **3** and **4** are found to be 3.81 and 3.95 respectively. This indicates some amount of exchange interaction in the solid complex [30].

Table 5
EPR Data of the copper complexes.

Compound	$G_{||}$	$g_{\perp}$	Ground State	Geometry
[Cu^{II}(HL)Cl(CH_3OH)].CH_3OH (3)	2.2639	2.0710	$d_{x2\text{-}y2}$	Square Pyramidal
[Cu^{II}(HL)(H_2O)(CH_3OH)]ClO_4 (4)	2.2155	2.0562	$d_{x2\text{-}y2}$	Square Pyramidal

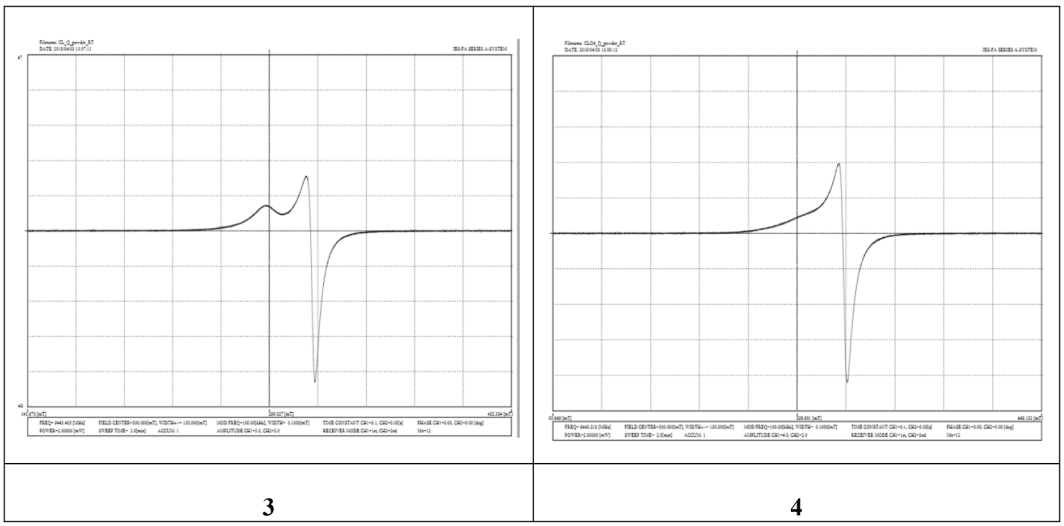

Fig. 4. EPR spectra of copper(II) complexes **3** and **4**.

The X-band EPR spectra of **3** and **4** were found with $g_{||} > g_{\perp}$ indicating the elongated distortion and the ground state electron lies in the $d_{x2\text{-}y2}$ orbital. The chloride and perchlorate complexes exhibited two 'g' values with square pyramidal geometries as $g_{||} > g_{\perp}$ and also supported by the crystallographic studies.

3.5. Biological assay

The ligands and their corresponding complexes were screened for antimicrobial and antituberculosis activities.

3.5.1. Antimicrobial activity studies

All the synthesized compounds were evaluated for their antimicrobial activity against gram-positive *S. aureus* bacterium, and gram-negative *E. coli* pathogens, using the micro broth dilution method. The result is tabulated in Table S8 and the analysis of the data is depicted in the Fig. 5**.** The copper perchlorate complex, **4** showed the lowest MIC of 0.4 μg/mL against the gram-positive, *S. aureus*, which was better than the ligand and the standard *Ciprofloxacin* drug. Whereas, the complexes **5** and **1** with 3.12 μg/mL and 6.25 μg/mL, respectively exhibited good activity, but for the rest, the MIC was as high as 25 μg/mL. In general, the ligand **H_2L** and its complexes exhibited better activity against gram-negative *E. coli* rather than the gram-positive *S. aureus*. The copper complex, **4** and the cobalt complex, **1** exhibited an MIC of 0.8 μg/mL, the nickel complex, **2** and zinc complex, **5** had shown much lower MIC of 0.4 μg/mL against *E. Coli*. However, **3** was active only at the MIC of 6.25 μg/mL. The major hurdle for all the antimicrobial drugs to act upon the microorganisms is to enter into their cells. The cell-membrane made up of the lipid bilayer acts as the protective shields to them. The antimicrobials act either by rupturing the cell-membrane or by interacting with the specific bio-molecules, especially enzymes in the cytoplasm. The permeability of the cell membrane depends upon various physicochemical features of the chemical drug species, like: lipophilicity, size, charge, solubility, and dissolution [41]. The observed activities of metal complexes synthesized by us, against the *in-vitro* studies on both the gram-positive and gram-negative microorganisms are intuitively assigned to their increased lipophilicity. The present quinolone hydrazone ligand moiety acquires sufficient amphiphilicity due to the non-polar nature of the aromatic rings comprising *t*-butyl groups, whereas the quinolone and aroylhydrazone parts consisting azomethine and other hetero atoms provide the essential polarities to the molecule. The amphiphilicity of the ligand enhances the membrane permeability, as well as the polar cites assist in binding to the cellular enzymes [42]. The coordination through chelation reduces the polarity of the metal ions by increasing the metal–ligand covalency, and enhances the lipophilicity of the central metal atom, there by favours the lipid-membrane permeability. However, comparatively higher MIC of the nickel complex **2**, cannot be clearly understood. Although, the gram-negative bacteria are said to possess stronger impermeable outer membranes [43] compared to that of gram-positive bacteria, in our case, ligand **H_2L** and almost all of its complexes exhibited specifically higher activities with lower MIC values against *E. Coli.* for unknown reasons. The complex **4,** is cationic with ClO_4^- being present outside the coordination sphere, whereas, chlorine occupies the axial position in the complex **3,** and is a neutral complex. The positive charge on the complex **4**, might be the reason for the higher activity of this complex against both the gram-positive and gram-negative pathogens [41].

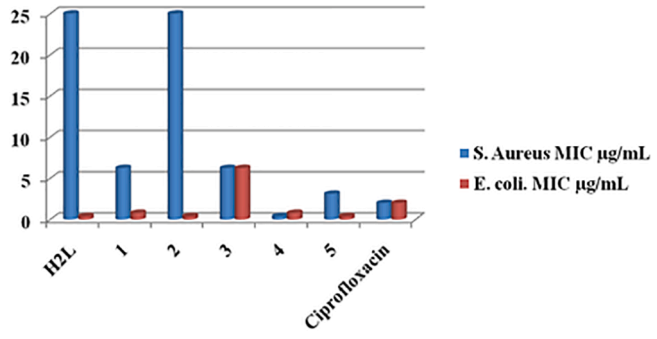

Fig. 5. MIC of H_2L and the complexes **1**–**5** against *S. Aureus* and *E. coli*. respectively.

3.5.2. Antitubercular activity

The synthesized compounds were also evaluated for their anti-mycobacterial activities against *M. tuberculosis* (H37RV strain): ATCC No-27294, using the Microplate Alamar Blue Assay (MABA) method. The results of the analysis are tabulated in Table S9, and the analysis of the data is depicted in the Fig. 6**.** The results indicated the MIC values of 6.25 μg/mL for the copper chloride **3** and perchlorate **4** complexes and were better than the ligand and as good as the standard Streptomycin drug. The other complexes **1**, **2**, and **5** were only as active as the ligand with the MIC of 25 μg/mL. The better anti-TB activities of the complexes **3** & **4**, could be readily associated to the copper coordination centre in both the compounds. Several reports [44,45] suggest that the redox activity of copper ions coupled with the bio-genicity, provides multiple mechanisms for the copper coordination complexes to act as better

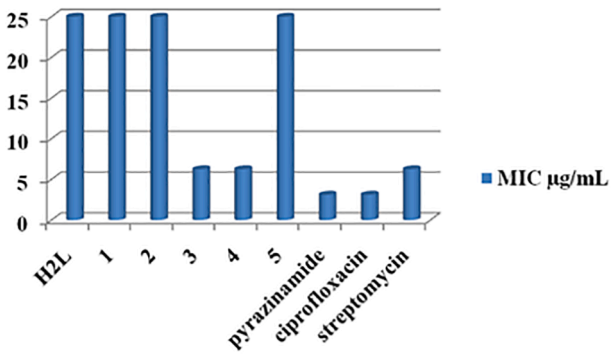

Fig. 6. AntiTB MIC evaluation of H_2L and complexes **1**–**5**.

antimicrobial and antitubercular agents.

4. Conclusion

The ligand 3,5-di-*tert*-butyl-2-hydroxy-*N*'-((2-oxo-1,2-dihydroquinolin-3-yl)methylene)benzohydrazide (**H_2L**) and its Co(II), Ni(II), Cu(II) and Zn(II) complexes were synthesized and structurally characterized. Further, the ligand behaves as monobasic and binds the metal (II) ion through the quinolone-carbonyl-O, imine-N and amidic enolate-O coordination sites in the tridentate manner. The cobalt and the nickel complexes, **1** and **2** were found to be octahedral neutral complexes with the general formula $[M^{II}(HL)_2]$ (where M = Co, Ni) and both were crystallized in the monoclinic crystal system with *C*2/*c* space groups. The two different copper complexes with the molecular formulae $[Cu^{II}(HL)Cl(CH_3OH)].CH_3OH$ (**3**) and $[Cu^{II}(HL)(H_2O)(CH_3OH)]ClO_4$ (**4**) were resulted, when the copper(II) chloride and copper(II) perchlorate salts were used for the complexation. Both the square-pyramidal complexes were crystallized in the triclinic crystal system with *P*-1 space groups. The zinc(II) complex, **5** with the six coordination and 1:2; M:L ratio, was assigned with $[Zn^{II}(HL)_2]$ as its molecular formula. The synthesized compounds were evaluated for antimicrobial and antitubercular activities. The antitubercular activities revealed the MIC values of 6.25 µg/mL for the copper complexes **3** and **4,** and were better than the ligand and as good as the standard *Streptomycin* drug. The ligand and its complexes exhibited good activity against gram-negative, *E. coli* than the gram-positive *S. aureus*. The nickel(II) **2** and zinc(II) **5** complexes have shown much lower MIC of 0.4 µg/mL against *E. coli*. The copper complex **4** exhibited the lowest MIC of 0.4 µg/mL against *S. aureus*.

Declaration of Competing Interest

The authors declare that they have no known competing financial interests or personal relationships that could have appeared to influence the work reported in this paper.

Acknowledgments

G. S. Hegde is thankful to the University Grants Commission, New Delhi (U.G.C.) for providing financial assistance under the Minor Research Project program with the UGC approval Letter No. MRP(S)-0475/13-14/KAKA089/UGC-SWRO and M. E. S., M. M. Arts and Science College, Sirsi, Uttara Kannada, Karnataka, India, for the basic research facilities, respectively. S. S. Bhat thanks the Department of Chemistry, Karnatak University Dharwad for providing the research facilities. The authors are thankful to USIC, Karnatak University, Dharwad, India, for providing spectral facilities. Recording of NMR from IOE-University of Mysore, EPR from SAIF IIT Bombay, biological activity studies from Maratha Mandal's Institute of Dental Science & Research Centre, Belgaum, SXRD analysis from CIF IISER Bhopal, India, and STIC Cochin are gratefully acknowledged.

Appendix A. Supplementary data

Supplementary data to this article can be found online at https://doi.org/10.1016/j.ica.2021.120352.

References

[1] A. Dömling, Chem. Rev. 106 (2006) 17–89.
[2] M.C. Mandewale, U.C. Patil, S.V. Shedge, U.R. Dappadwad, R.S. Yamgar, Beni-Suef University J. Basic Appl. Sci. 6 (2017) 354–361.
[3] M.C. Mandewale, B. Thorat, Y. Nivid, R. Jadhav, A. Nagarsekar, R. Yamgar, J. Saudi Chem. Soc. 22 (2018) 218–228.
[4] M. Dinakaran, P. Senthilkumar, P. Yogeeswari, A. China, V. Nagaraja, D. Sriram, Bioorg. Med. Chem. 16 (2008) 3408–3418.
[5] A. Lilienkampf, J. Mao, B. Wan, Y. Wang, S.G. Franzblau, A.P. Kozikowski, J. Med. Chem. 52 (2009) 2109–2118.
[6] S. Jayaprakash, Y. Iso, B. Wan, S.G. Franzblau, A.P. Kozikowski, ChemMedChem 1 (2006) 593–597.
[7] A. Nayyar, V. Monga, A. Malde, E. Coutinho, R. Jain, Bioorg. Med. Chem. 15 (2007) 626–640.
[8] L. Savini, L. Chiasserini, A. Gaeta, C. Pellerano, Bioorg. Med. Chem. 10 (2002) 2193–2198.
[9] M. Fleck, M. Layek, R. Saha, D. Bandyopadhyay, Transit. Metal Chem. 38 (2013) 715–724.
[10] S. Sain, R. Saha, G. Mostafa, M. Fleck, D. Bandyopadhyay, Polyhedron 31 (2012) 82–88.
[11] R. Musiol, J. Jampilek, V. Buchta, L. Silva, H. Niedbala, B. Podeszwa, A. Palka, K. Majerz-Maniecka, B. Oleksyn, J. Polanski, Bioorg. Med. Chem. 14 (2006) 3592–3598.
[12] I.A.M. Radini, T.M.Y. Elsheikh, E.M. El-Telbani, R.E. Khidre, Molecules 21 (2016) 909.
[13] C. Fernández-Galleguillos, L.A. Saavedra, M. Gutierrez, J. Braz. Chem. Soc. 25 (2014) 365–371.
[14] A. Marella, O.P. Tanwar, R. Saha, M.R. Ali, S. Srivastava, M. Akhter, M. Shaquiquzzaman, M.M. Alam, Saudi Pharm. J. 21 (2013) 1–12.
[15] V.R. Solomon, H. Lee, Curr Med Chem 18 (2011) 1488–1508.
[16] Z.-C. Liu, B.-D. Wang, Z.-Y. Yang, Y. Li, D.-D. Qin, T.-R. Li, Eur. J. Med. Chem. 44 (2009) 4477–4484.
[17] B.S. Creaven, B. Duff, D.A. Egan, K. Kavanagh, G. Rosair, V.R. Thangella, M. Walsh, Inorg. Chim. Acta 363 (2010) 4048–4058.
[18] C.-R. Li, Z.-C. Liu, B.-D. Wang, T.-R. Li, Z.-Y. Yang, Synth. Met. 209 (2015) 273–278.
[19] G.S. Hegde, S.P. Netalkar, V.K. Revankar, Appl. Organometal. Chem. 33 (2019), e4840.
[20] Bruker, SMART, SAINT and SADABS. Bruker AXS Inc., Madison, Wisconsin, USA (2007).
[21] O.V. Dolomanov, L.J. Bourhis, R.J. Gildea, J.A.K. Howard, H. Puschmann, J. Appl. Crystallogr. 42 (2009) 339–341.
[22] G. Sheldrick, Acta Crystallogr. A 71 (2015) 3–8.
[23] A. Spek, J. Appl. Crystallogr. 36 (2003) 7–13.
[24] Antimicrobial Susceptibility Testing Protocols, Taylor & Francis Group, Boca Raton, 2007.
[25] M. Masalha, I. Borovok, R. Schreiber, Y. Aharonowitz, G. Cohen, J. Bacteriol. 183 (2001) 7260.
[26] C. Elamathi, R. Butcher, R. Prabhakaran, Appl. Organometal. Chem. 33 (2019), e4659.
[27] D. Senthil Raja, N.S.P. Bhuvanesh, K. Natarajan, Inorg. Chem. 50 (2011) 12852–12866.
[28] R.K. Ray, G.B. Kauffman, Inorg. Chim. Acta 174 (1990) 257–262.
[29] R.A. Ammar, A.-N.-M.-A. Alaghaz, A.S. Alturiqi, Appl. Organometal. Chem. 32 (2018), e4361.
[30] P. Domiano, C. Pelizzi, G. Predieri, C. Vignalli, G. Palla, Polyhedron 3 (1984) 281–286.
[31] C. Amari, C. Pelizzi, G. Pelizzi, G. Predieri, G. Sartori, Inorg. Chim. Acta 223 (1994) 97–102.
[32] G.H. Chimmalagi, U. Kendur, S.M. Patil, K.B. Gudasi, C.S. Frampton, M.B. Budri, C. V. Mangannavar, I.S. Muchchandi, Appl. Organometal. Chem. 32 (2018), e4337.
[33] V. Vrdoljak, G. Pavlović, T. Hrenar, M. Rubčić, P. Siega, R. Dreos, M. Cindrić, RSC Adv. 5 (2015) 104870–104883.
[34] E. Ramachandran, V. Gandin, R. Bertani, P. Sgarbossa, K. Natarajan, N.S. P. Bhuvanesh, A. Venzo, A. Zoleo, A. Glisenti, A. Dolmella, A. Albinati, C. Marzano, J. Inorg. Biochem. 182 (2018) 18–28.
[35] A.W. Addison, T.N. Rao, J. Reedijk, J. van Rijn, G.C. Verschoor, J. Chem. Soc., Dalton Trans. 1349–1356 (1984).
[36] D. Moon, S. Tanaka, T. Akitsu, J.-H. Choi, J. Mol. Struct. 1154 (2018) 338–347.
[37] U. Kendur, G.H. Chimmalagi, S.M. Patil, K.B. Gudasi, C.S. Frampton, Appl. Organometal. Chem. 32 (2018), e4278.
[38] V. Kamat, V. Revankar, Inorg. Chim. Acta 476 (2018) 77–82.
[39] F.A. Cotton, G. Wilkinson, Advanced Inorganic Chemistry Ch-21 (1980) p-787..
[40] D. Kivelson, R. Neiman, J. Chem. Phys. 35 (1961) 149.
[41] Z. Liu, S. Wang, M. Hu, Developing Solid Oral Dosage Forms, Y. Qiu, Y. Chen, G.G. Z. Zhang, L. Liu, W.R. Porter (Eds.) Oral Absorption Basics: Pathways, Physicochemical and Biological Factors Affecting Absorption, (2009). Chapter 11, p. 265-288.

[42] N.S. Sara, Z. Fabio, Chemistry 2 (2020) 418–452.
[43] D.A.C. Heesterbeek, N.I. Martin, A. Velthuizen, M. Duijst, M. Ruyken, R. Wubbolts, S.H.M. Rooijakkers, B.W. Bardoel, Sci. Rep. 9 (2019) 3074.
[44] D. S. Joshi S, Gadag S, Kulkarni V, Aminabhavi T., Research and Reports, Med. Chem. 6 (2016) 1–14.
[45] P.B. da Silva, P.C. de Souza, G.M.F. Calixto, E.D.O. Lopes, R.C.G. Frem, A.V. G. Netto, A.E. Mauro, F.R. Pavan, M. Chorilli, Int. J. Mol. Sci. 17 (2016) 745.